

HIGH ENERGY ELASTIC pp SCATTERING IN ADDITIVE QUARK MODEL

Yu.M. Shabelski and A.G. Shuvaev

Petersburg Nuclear Physics Institute, Kurchatov National Research Centre
Gatchina, St. Petersburg 188300, Russia

E-mail: shabelsk@thd.pnpi.spb.ru

E-mail: shuvaev@thd.pnpi.spb.ru

Abstract

High energy pp and $p\bar{p}$ elastic scattering is treated in the framework of Additive Quark Model. The reasonable agreement with experimental data is achieved with the natural parameters for the strong matter distribution inside proton.

PACS. 25.75.Dw Particle and resonance production

1 Introduction

Regge theory provides a useful tool for the phenomenological description of high energy hadron collisions [1, 2, 3, 4, 5, 6, 7]. The quantitative predictions of Regge calculus are essentially dependent on the assumed coupling of participating hadrons to Pomeron. In this paper high energy elastic pp and $p\bar{p}$ scattering data including the recent LHC ones are analyzed in terms of the simple Regge exchange approach in the framework of Additive Quark Model (AQM) [8, 9]. In AQM baryon is treated as a system of three spatially separated compact objects – constituent quarks. Each constituent quark is colored, has internal quark-gluon structure and finite radius that is much less than the radius of proton, $r_q \ll r_p$. This picture is in good agreement both with $SU(3)$ symmetry of strong interaction and the quark-gluon structure of proton [10, 11].

The three constituent quarks are assumed in AQM to be the incident particles in pp or $p\bar{p}$ scattering. Elastic amplitudes for the large energy $s = (p_1 + p_2)^2$ and the small momentum transfer t are dominated by the Pomeron exchange. We neglect the small difference in pp and $p\bar{p}$ scattering coming from the exchange of negative signature

Reggeons, Odderon (see e.g. [12] and references therein), ω -Reggeon etc, since their contribution is suppressed by s .

The single t -channel exchange results into s -channel amplitude of the constituent quarks scattering

$$M_{qq}^{(1)}(s, t) = \gamma_{qq}(t) \cdot \left(\frac{s}{s_0} \right)^{\alpha_P(t)-1} \cdot \eta_P, \quad (1)$$

where $\alpha_P(t) = \alpha_P(0) + \alpha'_P \cdot t$ is the Pomeron trajectory specified by the values of intercept, $\alpha_P(0)$, and slope, α'_P . The (positive) signature factor,

$$\eta_P = i - \tan^{-1} \left(\frac{\pi \alpha_P(t)}{2} \right),$$

determines the complex structure of the amplitude. The factor $\gamma_{qq}(t) = g_1(t) \cdot g_2(t)$ has the meaning of the Pomeron coupling to the beam and target particles, the functions $g_{1,2}(t)$ being the vertices of constituent quark-Pomeron interaction (filled circles in Fig. 1). As the same set of the Pomeron parameters $\Delta = \alpha_P(0) - 1$, α'_P and γ_{qq} describes proton and antiproton scattering, both pp and $p\bar{p}$ data have been commonly used to fix their values ¹.

The one-Pomeron exchange between two protons includes the sum over all possible exchanges between the quark pairs [8, 9]. Each term in the sum has a form (1) with the functions $g_{1,2}(t)$ attributed to the individual constituent quarks.

Due to factorization of longitudinal and transverse degrees of freedom the longitudinal momenta are integrated over separately in high energy limit. After this the transverse part of the quark distribution is actually relevant only. Writing the proton wavefunction in the transverse momentum space as $\psi(k_1, k_2, k_3)$, where k_i are the quark transverse momenta,

$$\int |\psi(k_1, k_2, k_3)|^2 \delta^{(2)}(k_1 + k_2 + k_3) d^2k_1 d^2k_2 d^2k_3 = 1, \quad (2)$$

the proton - Pomeron vertex, $F_P(Q, 0, 0)$, $t = -Q^2$, is given by the overlap function

$$F_P(Q_1, Q_2, Q_3) = \int \psi^*(k_1, k_2, k_3) \psi(k_1 + Q_1, k_2 + Q_2, k_3 + Q_3) \times \delta^{(2)}(k_1 + k_2 + k_3) d^2k_1 d^2k_2 d^2k_3. \quad (3)$$

The function $F_P(Q, 0, 0)$ plays a role of the proton formfactor for strong interaction in AQM (see section 2).

¹Strictly speaking, exchange of the positive signature Reggeons determine half of the sum of pp and $p\bar{p}$ elastic amplitude. We neglect their difference.

In what follows we assume the Pomeron trajectory in the simplest form

$$\left(\frac{s}{s_0}\right)^{\alpha_P(t)-1} = e^{\Delta \cdot \xi} e^{-r_q^2 q^2}, \quad \xi \equiv \ln \frac{s}{s_0}, \quad r_q^2 \equiv \alpha' \cdot \xi.$$

The value r_q^2 defines the radius of quark-quark interaction while $S_0 = (9 \text{ GeV})^2$ has the meaning of typical energy scale in Regge theory. Putting together all 9 equal quark-quark contributions (one of them is shown in Fig. 1 a) we get the first order elastic pp (or $p\bar{p}$, we do not distinguish between them here) amplitude

$$M_{pp}^{(1)} = 9 \left(\gamma_{qq} \eta_P e^{\Delta \cdot \xi} \right) e^{-r_q^2 Q^2} F_P(Q, 0, 0)^2. \quad (4)$$

Actually the formula (4) with a single Pomeron gives amplitude in the impulse approximation [8]. Similarly to light nuclear scattering the multipomeron exchange should be added (see Glauber theory [13, 14]) giving rise to the terms $M_{pp}^{(2)}$, $M_{pp}^{(3)}$ etc, so that the total amplitude

$$M_{pp} = \sum_n M_{pp}^{(n)}.$$

If $r_q/r_p \rightarrow 0$ the multiple interactions become negligible leaving in the sum the first term only.

The optical theorem, that relates the total elastic cross section and imaginary part of the amplitude, in the normalization adopted here reads

$$\sigma_{pp}^{tot} = 8\pi \text{Im } M_{pp}(s, t=0).$$

The differential cross section is evaluated in this normalization as

$$\frac{d\sigma}{dt} = 4\pi |M_{pp}(s, t)|^2 = 4\pi [(\text{Re } M_{pp}(s, t))^2 + (\text{Im } M_{pp}(s, t))^2]. \quad (5)$$

Interference of the contributions generated by the various number of Pomerons leads to the occurrence of local minima in the differential elastic cross section. Experimentally the minimum at $t \simeq 0.53 \text{ GeV}^2$ for the energy $\sqrt{s} = 7 \text{ TeV}$ is well observed at LHC [18, 19]. The minima at another t are also possible. Basically there is interplay between the minima in real and imaginary parts of the amplitude in the expression (5) so that the minimum in the imaginary part could be filled by the large real part at the same t .

The present paper aims to give theoretical description of the experimental pp and $p\bar{p}$ elastic scattering data in the energy interval $546 \text{ GeV} \div 7 \text{ TeV}$ in the framework of AQM. The analysis of the differences in pp and $p\bar{p}$ amplitudes needs a more subtle treatment than that involving only Pomeron exchanges and goes beyond our approach.

2 Elastic Scattering Amplitude in AQM

In AQM there are a total 9 orders of interactions. The first order is the sum of all interactions between single qq pairs ² It contains 9 terms. Similar to Glauber theory [13, 14] one has to rule out the multiple interactions between the same quark pair. AQM permits the Pomeron to connect any two quark lines only once. It crucially decreases the combinatorics leaving the diagrams with no more than 9 effective Pomerons. Examples of various order diagrams are shown in Fig 1,2.

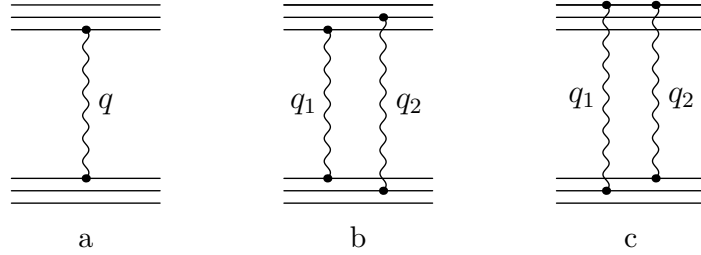


Figure 1: The AQM diagrams for pp elastic scattering. The straight lines stand for quarks, the waved lines denote Pomerons, Q is the momentum transferred, $t = -Q^2$. Diagram (a) is the one of the single Pomeron diagrams, diagrams (b) and (c) represent double Pomeron exchange with two Pomeron coupled to the different quark (b) and to the same quarks (c), $q_1 + q_2 = Q$.

Let q_i be the transverse momentum carried by the i -th effective Pomeron, Q_k and Q'_l denote the momenta transferred to the quark k from the target proton or quark l from the beam proton during the scattering process. If no Pomerons are attached to the quark j , that is it does not interact, then $Q_j = 0$. If only one Pomeron carrying momentum q_i is attached to the quark j , then $Q_j = q_i$. If two Pomerons with the momenta q_i and q_k are coupled to it, then $Q_j = q_i + q_k$. In other words,

$$Q_k = \sum q_i \text{ if Pomeron } i \text{ is attached to quark } k,$$

$$Q'_l = \sum q_{i'} \text{ if Pomeron } i' \text{ is attached to quark } l.$$

With these notations the n order amplitude is equal to

$$M^{(n)} = i^{n-1} \left(\gamma_{qq} \eta_{PE} \Delta \cdot \xi \right)^n \int \frac{d^2 q_1}{\pi} \dots \frac{d^2 q_n}{\pi} \pi \delta^{(2)}(q_1 + \dots + q_n - Q) \\ \times e^{-r_q^2(q_1^2 + \dots + q_n^2)} \frac{1}{n!} \sum_{n \text{ connections}} F_P(Q_1, Q_2, Q_3) F_P(Q'_1, Q'_2, Q'_3), \quad (6)$$

²Note that one qq pair interaction in AQM may include the contributions of several Gribovs' Pomerons [20]. We assume that high energy qq scattering is described by single effective Pomeron exchange between each qq pair, the parameters of this effective Pomeron could be different from those of Gribov's bare Pomerons.

where the sum in the last factor is taken over all distinct ways to connect the pairs of beam and target quarks by n effective Pomerons, each pair being connected no more than once. The permutations of identical Pomerons in the integrals is compensated by $1/n!$ in front the sum.

There are two types of diagrams in the second order,

$$\begin{aligned} & \frac{1}{2!} \sum_{2 \text{ connections}} F_P(Q_1, Q_2, Q_3) F_P(Q'_1, Q'_2, Q'_3) \\ &= 18 F_P(q_1, q_2, 0) F_P(q_1, q_2, 0) + 18 F_P(Q, 0, 0) F_P(q_1, q_2, 0), \quad Q = q_1 + q_2, \end{aligned}$$

where the first term comes from the diagrams with both Pomerons coupled to the different quark lines whereas in the second one they are attached to the same line (Fig. 1 b,c).

The third order sum is

$$\begin{aligned} & \frac{1}{3!} \sum_{3 \text{ connections}} F_P(Q_1, Q_2, Q_3) F_P(Q'_1, Q'_2, Q'_3) \\ &= 6 F_P(Q, 0, 0) F_P(q_1, q_2, q_3) + 9 F_P(q_1 + q_2, 0, q_3) F_P(q_1 + q_3, 0, q_2) \\ & \quad + 9 F_P(q_1 + q_2, 0, q_3) F_P(q_2 + q_3, 0, q_1) + 6 F_P(q_1 + q_2, 0, q_3) F_P(q_1, q_3, q_2) \\ & \quad + 18 F_P(q_1 + q_3, 0, q_2) F_P(q_2 + q_3, 0, q_1) + 15 F_P(q_1 + q_3, 0, q_2) F_P(q_1, q_3, q_2) \\ & \quad + 15 F_P(q_2 + q_3, 0, q_1) F_P(q_1, q_3, q_2) + 6 F_P(q_3, q_2, q_1) F_P(q_1, q_2, q_3), \end{aligned}$$

$$Q = q_1 + q_2 + q_3.$$

Here the first term arises when all three Pomerons are attached to the same line, in the last term they connect three different quarks, diagrams (a) and (d) in the Fig. 2. The second and the third terms correspond to the diagrams (b) and (c). The rest terms are provided by various permutations of the Pomeron lines in these diagrams, in particular, by flipping a diagram as a whole. The numerical coefficients encounter the

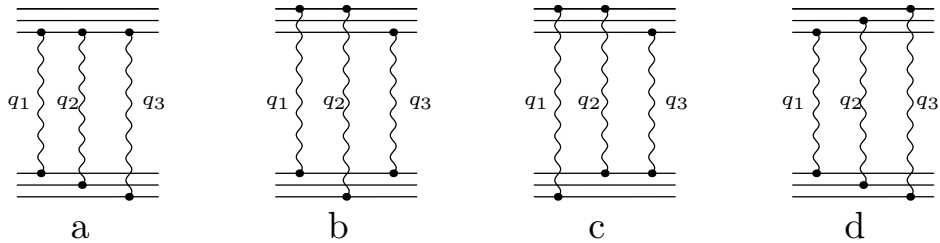


Figure 2: Several AQM diagrams of the third order.

number of connections resulting into equal expressions after variables changing in the integrals (6).

In the highest order, containing 9 effective Pomerons,

$$\frac{1}{9!} \sum_{9 \text{ connections}} F_P(Q_1, Q_2, Q_3) F_P(Q'_1, Q'_2, Q'_3)$$

$$= F_P(q_1 + q_2 + q_3, q_4 + q_5 + q_6, q_7 + q_8 + q_9) F_P(q_1 + q_4 + q_7, q_2 + q_5 + q_8, q_3 + q_6 + q_9),$$

each quark from the beam proton interacts with the quark from the target one. The other orders, $3 < n < 9$, have similar but more lengthly structure due to large combinatorics to redistribute q_1, \dots, q_n momenta among Q_i and Q'_i groups³.

The function $F_P(q_1, q_2, q_3)$ is determined by the proton wavefunction in terms of the constituent quarks (3). We model the transverse part of the wavefunction in a simple form of two gaussian packets,

$$\psi(k_1, k_2, k_3) = N[e^{-a_1(k_1^2 + k_2^2 + k_3^2)} + C e^{-a_2(k_1^2 + k_2^2 + k_3^2)}], \quad (7)$$

normalized to unity (2). One packet parametrization, $C = 0$, is insufficient to reproduce experimental data as imposing too strong mutual dependence between the total cross section, the minimum position and the value of the slope at $t = 0$.

All parameters used in the calculation naturally fall into two different kinds: the parameters of the Pomeron and those specifying the structure of colliding particles. The former type, Δ , α' , γ_{qq} , refers to the high energy scattering theory while the latter, $a_{1,2}$ and C , details the matter distribution inside the proton in the low energy limit(similar to density distribution in atomic nuclear).

With the chosen values of $a_{1,2}$ and C (see below) the wavefunction (7) results into the density shown in Fig. 3 It looks rather naturally having mean squared radius $\sqrt{\langle r^2 \rangle} = 0.68$ fm, that is close to the electromagnetic radius. Some discrepancy can be explained by the difference in the distributions of charged and strong interacting matter inside the proton.

3 Comparison with the experimental data

Here we present the numerical results obtained by summing over all 9 orders of interaction of the Additive Quark Model for the energies in the interval $\sqrt{s} = 546$ GeV \div

³The full set of similar diagrams for pp and $\alpha\alpha$ scattering can be found in ([15, 16]).

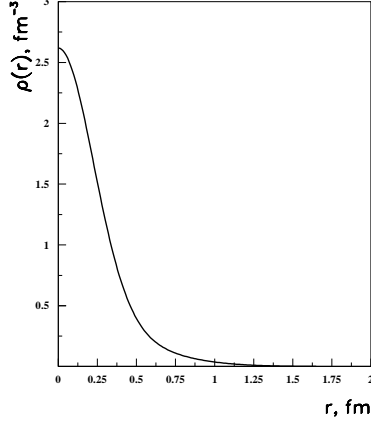


Figure 3: The radial density distribution in the proton calculated with the wavefunction (7) and parameters (8).

7 TeV. They are compared with the experimental data taken from [18, 19, 23, 25, 26, 27, 28, 29]. The following set of parameters have been used

$$\begin{aligned} \Delta &= 0.107 & \alpha' &= 0.32 \text{ GeV}^{-2} & \gamma_{qq} &= 0.44 \text{ GeV}^{-2} \\ a_1 &= 4.8 \text{ GeV}^{-2} & a_2 &= 0.87 \text{ GeV}^{-2} & C &= 0.132 \end{aligned} \quad (8)$$

In choosing these values we have not distinguished pp and $p\bar{p}$ data.

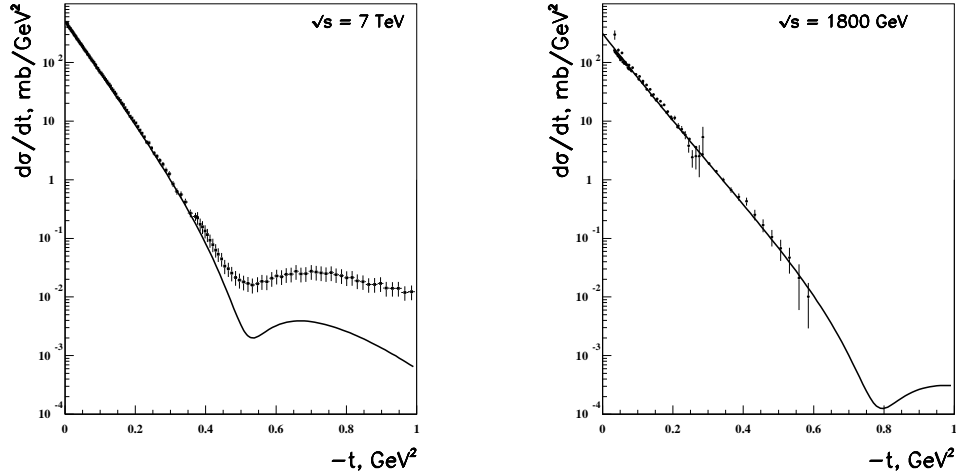


Figure 4: The differential cross section of elastic pp scattering at $\sqrt{s} = 7$ TeV and $p\bar{p}$ scattering at $\sqrt{s} = 1800$ GeV. The experimental points have been taken from [25, 29, 17, 18, 19].

The calculated values of the total cross section σ^{tot} , of $d\sigma/dt(t=0)$, of the slope of the elastic cross section B ($d\sigma/dt \sim \exp(-B \cdot t)$), and of the ratio $\rho = \text{Re } \sigma / \text{Im } \sigma(t=0)$

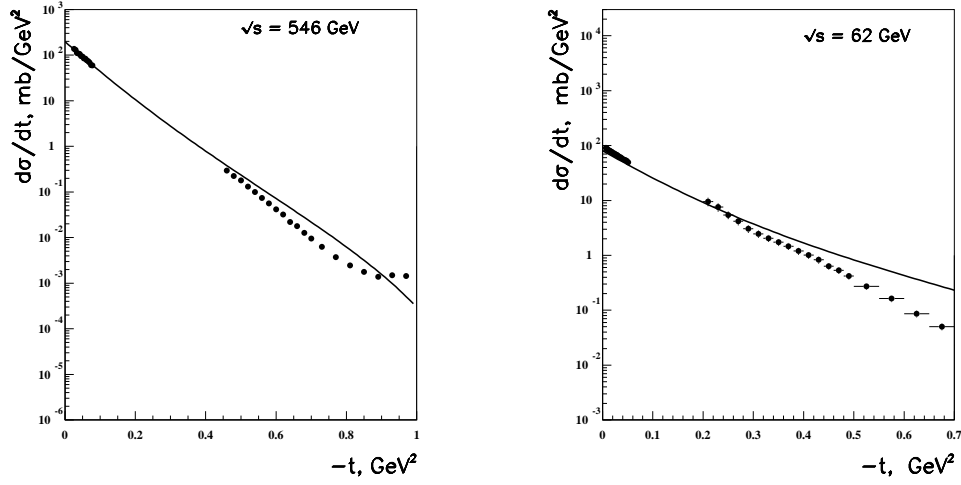


Figure 5: The differential cross section of elastic $p\bar{p}$ scattering at $\sqrt{s} = 546$ GeV and elastic pp scattering at $\sqrt{s} = 62$ GeV. The experimental points have been taken from [25, 26] (left panel), [23] for $p\bar{p}$ and [27] for pp (right panel).

are presented in the Table 1 along with the experimental data. The theoretical slope is calculated within the interval $|t| = 0 - 0.1$ GeV². Here we again neglect the difference between pp and $p\bar{p}$ collisions in the presented data.

\sqrt{s}	σ^{tot} (mb)	$d\sigma/dt(t=0)$ (mb/GeV ²)	B (GeV ⁻²)	$\text{Re } \sigma / \text{Im } \sigma$ ($t = 0$)
7 TeV	98.54	500.32	20.16	0.099
[17]	98.3 ± 2.8	-	$20.1 \pm 0, 4$	-
1.8 TeV	77.58	310.48	17.33	0.104
[25]	-	334.6 ± 18.8	$16.98 \pm 0, 25$	-
546 GeV	62.06	198.84	15.09	0.11
[24]	-	-	-	0.135 ± 0.015
[25]	-	196.1 ± 6	$15.35 \pm 0, 19$	-
62 GeV	39.54	80.73	11.46	0.11
[23]	43.55 ± 0.31	-	13.02 ± 0.27	-
[28]	-	-	13.3 ± 0.3	0.095 ± 0.011

Table 1. The comparison of the calculated values of total cross sections σ^{tot} , of $d\sigma/dt(t=0)$, slope parameter B and ratio $\text{Re } \sigma / \text{Im } \sigma(t=0)$ with the available experimental data.

The values of the total cross sections and the slopes are in reasonable agreement with the experimental data, the value $\rho = \text{Re } \sigma / \text{Im } \sigma(t=0)$ is also well reproduced at

$\sqrt{s} = 546$ GeV. The AQM assumption $r_q^2 \ll r_p^2$ continues to hold satisfactorily even at the LHC energy $\sqrt{s} = 7$ TeV for $r_q^2 \simeq 5$ GeV $^{-2}$, $r_p^2 \simeq 12$ GeV $^{-2}$. Probably it would be better fulfilled if the Pomeron slope α' would be lesser. The value obtained for the total cross section for $p\bar{p}$ scattering at $\sqrt{s} = 62$ GeV are smaller than the experimental data. The reason might be in non-Pomeron contributions, for example in f Reggeon, whose effect could be significant for the low energies but disappears when the energy grows.

The experimental position of the local minimum of the differential pp cross section at $\sqrt{s} = 7$ TeV is also reproduced although the theory predicts the more deep minimum. As the transferred momentum increases, $|t| \geq 1$ GeV 2 , the interaction becomes sensitive to the internal structure of constituent quarks that have a finite size. We have used a simple parametrization for their radius $r_q^2 = \alpha'\xi$, but there is a possibility for additional constants or more complicated functions. The experimental data for $p\bar{p}$

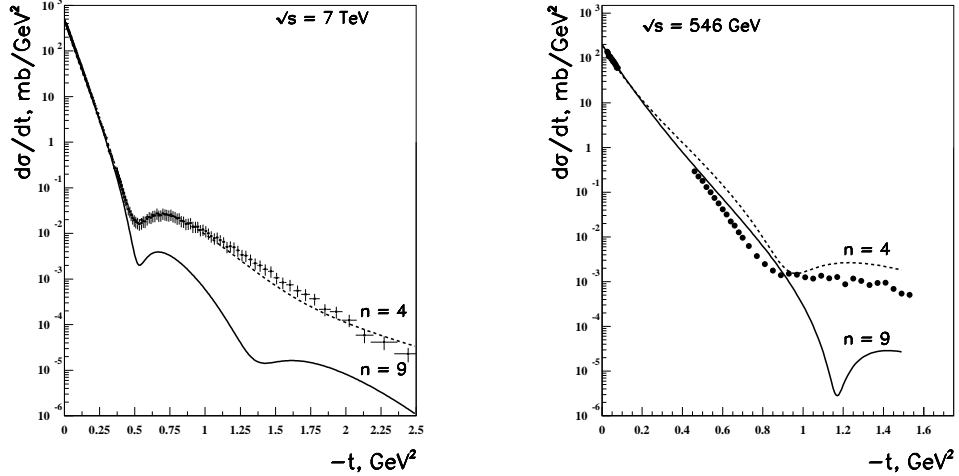


Figure 6: The differential cross section of elastic pp scattering at $\sqrt{s} = 7$ TeV (left panel) and elastic $p\bar{p}$ scattering at $\sqrt{s} = 546$ GeV (right panel). The dashed line ($n = 4$) presents the sum of first four orders of AQM calculated with the parameters $\Delta = 0.1$, $\alpha' = 0.38$ GeV $^{-2}$, $\gamma = 0.45$ GeV $^{-2}$, $a_1 = 6.5$ GeV $^{-2}$, $a_2 = 0.47$ GeV $^{-2}$, $C = 0.081$. The solid line ($n = 9$) presents the sum of all AQM orders for the parameters (8). It exhibits the second local minimum for pp scattering at $\sqrt{s} = 7$ TeV. The experimental points have been taken from [17, 18, 19, 25, 26]

scattering show no clean dips at the smallest energies $\sqrt{s} = 1800$ GeV, 546 GeV and 62 GeV. The reason, probably, is in substantial contribution that could be made to $p\bar{p}$ amplitude by the negative signature Reggeons (see Conclusion).

It is important to note that the complete 9 orders AQM calculation yields a second local minimum of the differential elastic pp cross section at $\sqrt{s} = 7$ TeV for

$|t| \geq 1 \text{ GeV}^2$ unobservable experimentally. It may indicate to an invalidity of our description for $|t| > 1 \text{ GeV}^2$, where the internal structure of the constituent quarks becomes important. From another point of view there is an uncontrolled contribution of multipomeron diagrams, (e.g. enhanced Pomeron diagrams [20]) rapidly growing with the number of Pomerons. Their numerical value is determined by unknown vertices of $m \rightarrow n$ Pomeron transitions, which increases the uncertainty of the next orders. In this context, it is worth stressing that the sum of only first four orders of AQM results (with a little modified parameters) into the theoretical curve that better fits the LHC pp data at the more broad t interval and does not exhibit an extra local minimum as is shown in Fig. 6 left.

An example of AQM predictions for $p\bar{p}$ scattering in the region $|t| \geq 1 \text{ GeV}^2$ for the energy $\sqrt{s} = 546 \text{ GeV}$ is presented in Fig. 6 right. The theory gives here the large dip, which is in fact absent in the experimental data. It points to the essential effect of the contributions, that are not accounted for in AQM, such as negative signature Reggeons etc. Nevertheless, the first four orders of AQM better describe the cross section behavior (give much smaller dip than the complete sum) even in this case. Both theoretical curves, $n = 4$ and $n = 9$, have no extra local minima up to $|t| \simeq 2.5 \text{ GeV}^2$ for this energy.

4 Conclusion

We show that the simple AQM model gives reasonable description of the high energy pp and $p\bar{p}$ elastic scattering at the not large momentum transferred, $|t| \leq 1 \text{ GeV}^2$, that is at the distances where the internal structure of the constituent quarks probably do not show up. Our model contains 6 parameters, but only 3 of them, $(\Delta, \alpha', \gamma_{qq})$, are employed to describe high energy scattering while 3 others $(a_{1,2}, C)$ determine the matter distribution in the proton. Note that the first group of parameters refers to the Pomeron and has been chosen over together taken pp and $p\bar{p}$ data. The interesting fact is that the matter distribution cannot be parameterized by one Gaussian packet (see also [6]).

As mentioned in the Introduction we neglect the contribution of the negative signature Reggeons that leads to the difference in pp and $p\bar{p}$ scattering especially around the dip. Some difference between them is experimentally observed [30, 31] at $\sqrt{s} = 53 \text{ GeV}$ near the dip ($|t| > 1 \text{ GeV}^2$). The energy behavior of this difference depends on the value of the Odderon intercept, α_{Odd} . The same Odderon effects are responsible for the difference in p and \bar{p} yields in the central region of the pp collision. However, it was shown [32, 33] that the observed ratio \bar{p}/p is compatible with the value $\alpha_{\text{Odd}} \sim 0.5$. In

this case the difference in $d\sigma/dt$ for pp and $p\bar{p}$ scattering should very fast decrease with the initial energy growth and seems to be very small at LHC. As a consequence the dip in the differential cross section clearly observed at LHC energy for pp scattering should manifest itself in $p\bar{p}$ scattering as well. It can be considered as our prediction.

A detailed study of peculiar features that distinguish pp and $p\bar{p}$ scattering needs a more careful analysis, which is beyond the framework of this paper.

The authors are grateful to M.G. Ryskin for helpful discussion.

This work has been supported by RSCF grant No 14 - 22 - 00281.

References

- [1] I. M. Dremin, Phys. Usp. **56** (2013) 3 [Usp. Fiz. Nauk **183** (2013) 3] [arXiv:1206.5474 [hep-ph]].
- [2] M. G. Ryskin, A. D. Martin and V. A. Khoze, Eur. Phys. J. C **72** (2012) 1937
- [3] V. A. Khoze, A. D. Martin and M. G. Ryskin, Eur. Phys. J. C **73** (2013) 2503 [arXiv:1306.2149 [hep-ph]].
- [4] E. Gotsman, E. Levin and U. Maor, Phys. Lett. B **716** (2012) 425 [arXiv:1208.0898 [hep-ph]].
- [5] E. Gotsman, E. Levin and U. Maor, Phys. Rev. D **85** (2012) 094007 [arXiv:1203.2419 [hep-ph]].
- [6] C. Merino and Y. .M. Shabelski, JHEP **1205** (2012) 013 [arXiv:1204.0769 [hep-ph]].
- [7] O. V. Selyugin, Eur. Phys. J. C **72** (2012) 2073 [arXiv:1201.4458 [hep-ph]].
- [8] E. M. Levin and L. L. Frankfurt, JETP Lett. **2** (1965) 65.
- [9] J. J. J. Kokkedee and L. Van Hove, Nuovo Cim. **42** (1966) 711.
- [10] Y. L. Dokshitzer, D. Diakonov and S. I. Troian, Phys. Rept. **58**, 269 (1980).
- [11] V. M. Shekhter, Yad.Fiz. **33** (1981) 817; Sov. J. Nucl. Phys. **33** (1981) 426.
- [12] R. Avila, P. Gauron and B. Nicolescu, Eur. Phys. J. C **49**, 581 (2007) [hep-ph/0607089].

- [13] R. J. Glauber. In "Lectures in Theoretical Physics", Eds. W. E. Brittin et al., New York (1959), vol.1, p.315.
- [14] V. Franco and R. J. Glauber, Phys.Rev. **142** (1966) 1195.
- [15] A. Bialas, K. Fialkowski, W. Slominski and M. Zielinski, Acta Phys. Polon. B **8** (1977) 855.
- [16] A. Bialas and A. Kolawa, Acta Phys. Polon. B **14** (1983) 539.
- [17] G. Antchev et al., TOTEM Collaboration, Europhys. Lett. **96**, 21002 (2011).
- [18] TOTEM Collaboration, G. Antchev et al., Europhys.Lett. **101** (2013) 21002.
- [19] TOTEM Collaboration, G. Antchev et al., Europhys.Lett. **95** (2011) 41001, [arXiv:1110.1385].
- [20] V.N. Gribov, Sov.Phys.JETP **56** (1969) 892.
- [21] M. Froissart, Phys. Rev. **123** (1961) 1053.
- [22] K.A. Ter-Martirosyan, Yad. Fiz. **10**, 1047 (1969).
- [23] N. A. Amos, M. M. Block, G. J. Bobbink, M. Botje, D. Favart, C. Leroy, F. Linde and P. Lipnik *et al.*, Nucl. Phys. B **262** (1985) 689.
- [24] C. Auger *et al.*, UA4/2 Collaboration, Phys. Lett. **B316**, 448 (1993).
- [25] F. Abe *et al.* [CDF Collaboration], Phys. Rev. D **50** (1994) 5518.
- [26] M. Bozzo *et al.* [UA4 Collaboration], Phys. Lett. B **155**, 197 (1985).
- [27] N. Kwak, E. Lohrmann, E. Nagy, M. Regler, W. Schmidt-Parzefall, K. R. Schubert, K. Winter and A. Brandt *et al.*, Phys. Lett. B **58** (1975) 233.
- [28] U. Amaldi et al., Phys. Lett. **B66**, 390 (1977).
- [29] N. A. Amos *et al.* [E-710 Collaboration], Phys. Lett. B **247** (1990) 127.
- [30] A. Breakstone, H. B. Crawley, G. M. Dallavalle, K. Doroba, D. Drijard, F. Fabbri, A. Firestone and H. G. Fischer *et al.*, Phys. Rev. Lett. **54** (1985) 2180.
- [31] S. Erhan, A. M. Smith, L. Meritet, M. Reyrolle, F. Vazeille, R. Bonino, A. Castellina and M. Medinnis *et al.*, Phys. Lett. B **152** (1985) 131.

- [32] K. Aamodt *et al.* [ALICE Collaboration], Phys. Rev. Lett. **105**, 072002 (2010).
- [33] C. Merino, M. M. Ryzhinskiy and Y. .M. Shabelski, Eur. Phys. J. C **62** (2009) 491.